Journal of Power Sources 250 (2014) 128–133

Contents lists available at ScienceDirect

Journal of Power Sources

journal homepage: www.elsevier.com/locate/jpowsour

Short communication

Pd oxides/hydrous oxides as highly efficient catalyst for formic acid electrooxidation

Liang Yan [a,c], Shikui Yao [a,c], Jinfa Chang [a], Changpeng Liu [b,*], Wei Xing [a,*]

[a] State Key Laboratory of Electroanalytical Chemistry, Changchun Institute of Applied Chemistry, 5625 Renmin Street, Changchun 130022, PR China
[b] Laboratory of Advanced Power Sources, Changchun Institute of Applied Chemistry, 5625 Renmin Street, Changchun 130022, PR China
[c] University of Chinese Academy of Sciences, Beijing, PR China

HIGHLIGHTS

- Annealing of Pd/C catalyst under the O_2 atmosphere produces POHOs.
- Improved mass activity and stability was obtained for FAEO.
- The introduction of POHOs significantly improves the performance of the DFAFCs.

ARTICLE INFO

Article history:
Received 3 May 2013
Received in revised form
15 October 2013
Accepted 19 October 2013
Available online 26 October 2013

Keywords:
Pd oxides/hydrous oxides
Direct formic acid fuel cells
Formic acid electrooxidation
Pd-based catalyst

ABSTRACT

A novel Pd-based catalyst for formic acid electrooxidation (FAEO) was prepared by annealing commercial Pd/C catalyst under the O_2 atmosphere at 100 °C, which exhibits excellent catalytic activity and stability for FAEO due to introduction of Pd oxides/hydrous oxides (POHOs). The catalytic activity of the as-prepared catalyst towards FAEO is 1.86 times of the commercial Pd/C catalyst in 0.5 M H_2SO_4 + 0.5 M HCOOH solution. Chronoamperometric curves show obvious improvement of the as-prepared catalyst electrocatalytic stability for FAEO. It is confirmed that POHOs can provide the required oxygen species for intermediate CO oxidation during the oxidation process of formic acid.

1. Introduction

Direct formic acid fuel cells (DFAFCs) have been attracting much attention as clean and high-efficiency energy conversion devices for portable electronic apparatus due to several attractive features, such as faster oxidation kinetics, less toxicity and lower crossover of formic acid through Nafion membrane than methanol etc. [1–3]. For the DFAFCs, Pd-based catalysts have commonly been used as the anode because of their higher catalytic activity for FAEO, lower cost, and greater abundance compared with Pt-based catalysts [2,4]. Although the Pd has been widely studied as the catalyst for FAEO, the limited durability of Pd-based catalysts for FAEO is still unsolved and hinders the practical application of DFAFCs [5,6]. The performance degradation of the DFAFCs is resulted from the agglomeration of Pd nanoparticles due to dissolution and redeposition process during DFAFC operation [6–8] and the poisoning of the anode. Possible adsorbed species, such as CO_{ad} [9] and –COOH [10], were considered as the reaction intermediates or the side products for FAEO, which causes the poisoning of the electrode and therefore performance loss of the DFAFCs.

Pd-based catalysts have been extensively employed for the FAEO, oxygen reduction reaction and alcohol electrooxidation [11–13]. Although Pd-based catalysts have better catalytic activity than Pt-based, the limited durability of Pd-based catalysts for FAEO is still the major challenges for the practical application of DFAFCs. Recently, improved catalytic activity for electrocatalysts by heat-treated in oxygen atmosphere has been investigated by many groups [14–19]. Huang et al. [14] found that the activity of the fresh PtRu/C catalyst was significantly improved by oxidation treatment. The variation in activity may be caused by changes in catalyst structure during oxidation treatment. The enhancement was attributed to the segregation of Ru and the formation of Ru^cO_2. Ren et al. [19] found that POHOs play a crucial role in increasing cell performance and minimizing performance degradation of the Pd-

* Corresponding authors. Tel.: +86 431 85262223; fax: +86 431 85685653.
E-mail addresses: liuchp@ciac.jl.cn (C. Liu), xingwei@ciac.jl.cn (W. Xing).

0378-7753/$ – see front matter © 2013 Elsevier B.V. All rights reserved.
http://dx.doi.org/10.1016/j.jpowsour.2013.10.085

based catalysts. The introduction of POHOs during electrocatalysis of FAEO is found to promote elimination of poisoning species, thereby leading to a better performance of the Pd-based catalysts. However, the Pd-based catalyst needs exposure in the air for ca. six months, which seems to be rather time consuming according to the report in the literature.

In present work, in order to obtain a high POHOs content in Pd/C catalysts in a short period of time for practical application, the commercial Pd/C catalysts were applied by an annealing treatment at a certain temperature in a tubular oven. The as-prepared catalysts exhibited much higher catalytic activity and much higher stability for FAEO than the commercial catalysts; the passive DFAFCs with the as-prepared catalysts have exhibited much higher cell performance and much better long-term stability than those with the commercial catalysts.

2. Experimental

2.1. Catalyst treatment

Commercial 30 wt.% Pd/C catalyst (Sigma–Aldrich, USA) denoted as Pd/C–C was used for comparison as a baseline catalyst. It was transferred and heated in a tubular oven at 100 °C under the O_2 atmosphere for 24 h, the temperature was ramped at a rate of 5 °C min^{-1} to the final temperature and the flow rate of O_2 was 80 cc min^{-1} to obtain the POHOs, the sample was denoted as Pd/C–O. The above-mentioned procedure was applied to fabricate the Pd/C–H catalyst, except that the annealing atmosphere was H_2.

2.2. Electrochemical measurements

All the electrochemical measurements were performed with an EG & G PARC potentiostat/galvanostat (Model 273A Princeton Applied Research Co., USA) and a conventional three-electrode electrochemical cell. A Pt foil and a saturated calomel electrode (SCE) were used as the counter and the reference electrodes, respectively. All potentials were referenced to SCE. The working electrode was prepared as follows. First, 5 mg of the catalyst was dispersed ultrasonically in 1000 μL of the alcohol solution containing 50 μL Nafion solution (5 wt.%, Aldrich Co., USA). Second, 5 μL of the above solution was pipetted and spread on a mirror-finished glassy carbon electrode with 4 mm diameter. At last, it was dried at room temperature for 30 min.

All electrochemical measurements were carried out in a 0.5 M H_2SO_4 solution with or without HCOOH deaerated by pure N_2 for at least 20 min prior to any measurements. For the electrooxidation of formic acid, the scan potential range was from −0.2 to +0.8 V. The CO_{ad} stripping voltammograms were measured in a 0.5 M H_2SO_4 solution. CO was purged into the 0.5 M H_2SO_4 solution for 15 min to allow the complete adsorption of CO onto the catalyst when the working electrode was kept at 0.2 V, and excess CO in the electrolyte was purged out with N_2 for 30 min. All the measurements were carried out at room temperature, unless otherwise noted. The surface area of Pd metal was estimated assuming that the coulombic charge necessary for oxidation of a monolayer of linearly adsorbed H was 210 μC cm^{-2} [20] while CO was 420 μC cm^{-2} [21,22].

2.3. Physical characterization

X-ray diffraction (XRD) measurements were performed with a PW-1700 diffractometer using a Cu K_α (λ = 1.5405 Å) radiation source (Philips Co.), the obtained XRD patterns were analyzed with Jade 5.0 software to remove the background radiation; X-ray photoelectron spectroscopy (XPS) measurements were carried out on Mg K_α radiation source (Kratos XSAM-800 spectrometer), the size and morphology of the catalysts were measured by transmission electron microscope (TEM) operating at 200 kV (Philips TECNAI G2).

2.4. MEA preparation

Preparation of membrane electrode assemblies (MEAs) [23]: A slurry consisted of Vulcan XC-72 carbon and PTFE (20 wt.%) was coated onto the carbon paper (TGPH030, 20 wt.% PTFE, Toray) to form the cathode diffusion layer. The Vulcan XC-72 carbon loading was ca. 2 mg cm^{-2}.

Commercial 30 wt.% Pd/C black (Sigma–Aldrich, USA) and Pt black (Johnson Matthey, USA) were used as catalysts in the anode and cathode, respectively. The catalyst ink mixed by the catalyst, ultrapure water, isopropyl alcohol and 5 wt.% Nafion® ionomer solution was sprayed onto the diffusion layer to fabricate the catalyst layers. The anode catalytic ink was directly sprayed onto the carbon paper (TGPH060, 20 wt.% PTFE, Toray). The noble metal loading was 4.0 mg cm^{-2} for both the anode and cathode. The Nafion ionomer loadings were 20 wt.% for anode and 15 wt.% for cathode. Then an additional layer of Nafion® ionomer with an amount of 0.1 g cm^{-2} was sprayed on the catalyst layer, it acts as an adhesion layer. The MEAs were prepared by hot-pressing both anode and cathode on both sides of a pretreated Nafion 115 proton exchange membrane at 135 °C and 3 MPa for 150 s. The above procedure was applied to fabricate other two MEAs, the difference is that the anode catalysts were heat-treated under the O_2 or H_2 for 24 h, while the former was not heat-treated.

2.5. Single cell assembly and measurement

The MEA performance was evaluated in a single cell with an active cross-section area of 4 cm^2. The single cell was measured at ambient conditions. A 10 M HCOOH solution was injected into a reservoir. The polarization and power density curves of the single cell were measured by a Fuel Cell Test System (Arbin Instruments Co.).

3. Results and discussion

3.1. Electrochemical analysis

Fig. 1 shows cyclic voltammograms (CVs) of the Pd/C–C, Pd/C–O, Pd/C–H catalysts in 0.5 M H_2SO_4 solution at the scan rate of

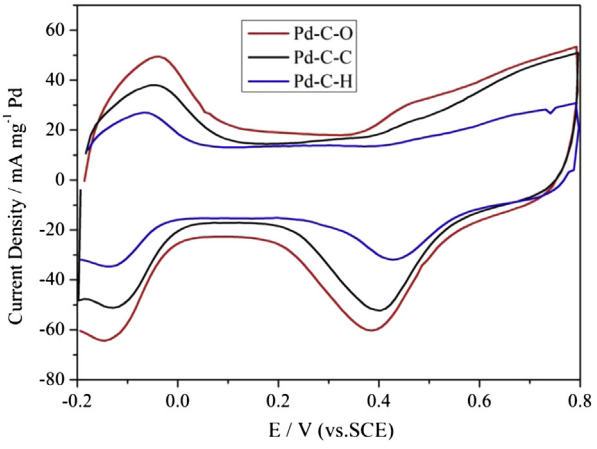

Fig. 1. CVs of different catalysts in 0.5 M H_2SO_4 solution with a scan rate of 50 mV s^{-1}.

50 mV s^{-1}. It is clear that all catalysts show expected behavior of Pd electrode in H_2SO_4 solution with well defined hydrogen adsorption/desorption (H_{ad}) peaks around −0.05 V and Pd oxide reduction peak in the reverse scan at ca. 0.45 V. All these features are typical for Pd catalysts in H_2SO_4 solution and agree well with the reported data [24–26]. Obviously, the Pd/C–O catalyst show higher peak area than Pd/C–C and Pd/C–H catalysts according to the area of the H_{ad} peaks of three catalysts, indicating that the Pd/C–O catalyst possess a larger electrochemical surface area (ECSA). The detailed data are shown in Table 1. The ECSA of the catalysts integrated from the H_{ad} shows an order of Pd/C–H < Pd/C–C < Pd/C–O.

CO_{ad} stripping, as a structure-sensitive measurement, was adopted to evaluate the difference in the resistance to CO and ECSA of different catalysts. CO_{ad} stripping voltammograms for different catalysts in 0.5 M H_2SO_4 solution with a scan rate of 50 mV s^{-1} are shown in Fig. 2. The surface areas of the three catalysts by integration of the CO_{ad} stripping peak are shown in Table 1, which give an order of Pd/C–H < Pd/C–C < Pd/C–O. Typically, the ECSA of Pd/C–O catalyst is 80.3 m^2 g^{-1}, which is 26% and 46% higher compared to the Pd/C–C (63.8 m^2 g^{-1}) and Pd/C–H (54.6 m^2 g^{-1}) catalysts. The peak potential (V) for CO_{ad} stripping for the three catalysts is also shown in Table 1, the Pd/C–C, Pd/C–O and Pd/C–H catalysts show primary CO_{ad} stripping peaks located at 0.715, 0.697 and 0.724 V, respectively. The oxidation peak and the onset potential for CO_{ad} oxidation for Pd/C–O catalyst shift negatively compared with Pd/C–C catalyst, indicating that the addition of oxygen facilitates the weakening of the CO adsorptive bond on the Pd active sites.

Fig. 3 displays the cyclic voltammograms (CVs) of different catalysts in 0.5 M H_2SO_4 + 0.5 M HCOOH solution at a scan rate of 50 mV s^{-1}. Clearly, the specific activities of the catalysts show an order of Pd/C–H < Pd/C–C < Pd/C–O. At 0.2 V [1], the Pd/C–O catalyst has 872 mA mg^{-1} Pd, which is significantly higher than the Pd/C–C (602 mA mg^{-1} Pd) and the Pd/C–H (381 mA mg^{-1} Pd) catalysts. The peak current density for Pd/C–O catalyst is 1142 mA mg^{-1} Pd, which is about 0.86 times higher than the Pd/C–C catalyst (613 mA mg^{-1} Pd) and 1.78 times higher than the Pd/C–H catalyst (410 mA mg^{-1} Pd). The specific activities in the CVs of different catalysts are shown in Fig. 4, which give an order of Pd/C–H < Pd/C–C < Pd/C–O. The Pd/C–O catalyst obtained by heat treatment in O_2 atmosphere displays the highest activity compared to the commercial Pd/C and the Pd/C–H catalysts. From this aspect, it is confirmed that the FAEO at the Pd/C–O catalyst is much easier than the commercial Pd/C catalyst. The current increase may be reasonably attributed to the existence of POHOs in the Pd catalysts [18,19].

Chronoamperometric curves were used to compare the electrocatalytic stabilities of different catalysts for FAEO. Fig. 5 shows the chronoamperometric curves of the three catalysts in 0.5 M H_2SO_4 solution containing 0.5 M HCOOH at 0.2 V for 3600 s. The results indicate that the current density of the Pd/C–O catalyst for FAEO is enhanced greatly comparing with other two catalysts, and the curves reach a steady state after about 3000 s. The current densities at 1000 s are 432, 277 and 150 mA mg^{-1} Pd for Pd/C–O, Pd/C–C and Pd/C–H catalysts, respectively. Even at 3600 s, the current density of Pd/C–O catalyst is still 228 mA mg^{-1} Pd, which is 1.56 times higher than Pd/C–C catalyst (89 mA mg^{-1} Pd) and 2.8 times higher than Pd/C–H catalyst (60 mA mg^{-1} Pd). The long-term poisoning rates (δ) are 73.43%, 87.01% and 90.12% or Pd/C–O, Pd/C–C and Pd/C–H catalysts, respectively. The above results indicate that the Pd/C–O catalyst has greatly enhanced catalytic activity and stability comparing with the commercial Pd/C and Pd/C–H catalysts for FAEO.

Table 1
ECSA integration from the H_{ad} and CO_{ad} stripping experiment and peak potential for CO_{ad} stripping for the three catalysts in 0.5 M H_2SO_4 solution with a scan rate of 50 mV s^{-1}.

Sample	Pd/C–C	Pd/C–O	Pd/C–H
ECSA[a] (m^2 g^{-1})	48.7	68.6	43.5
ECSA[b] (m^2 g^{-1})	63.8	80.3	54.6
Peak potential (V)	0.715	0.697	0.724

[a] The ECSA of the catalysts integration from the H_{ad} experiment.
[b] The ECSA of the catalysts integration from the CO_{ad} stripping experiment.

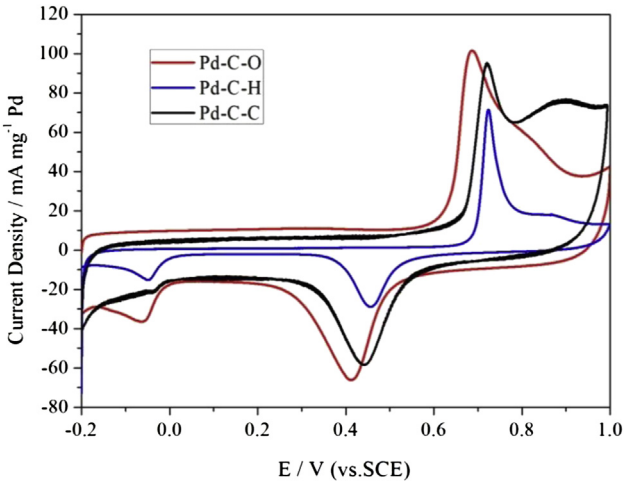

Fig. 2. CO_{ad} stripping voltammograms for different catalysts in 0.5 M H_2SO_4 solution with a scan rate of 50 mV s^{-1}.

3.2. Physical characterization

The XRD patterns of different catalysts are given in Fig. 6. All three catalysts show typical Pd fcc structure, with five characteristic diffraction peaks observed at 40.2°, 46.8°, 68.1°, 81.7°, 86.6°, corresponding to the (111), (200), (220), (311) and (222) crystal facets, respectively [27]. It should be noted that the XRD patterns for both the Pd/C–O and Pd/C–C catalysts display a diffraction peak at approximately 34° in Fig. 5, which can be ascribed to the presence of POHOs [19]. The greater POHOs peak intensity for the Pd/C–O catalyst comparing with the Pd/C–C and Pd/C–H catalysts indicates that the content of POHOs in Pd/C–O catalyst is higher than that of

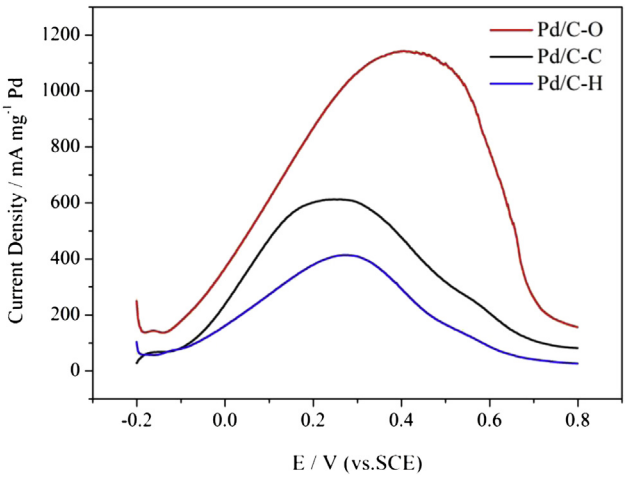

Fig. 3. CVs of different catalysts in 0.5 M H_2SO_4 + 0.5 M HCOOH solution with a scan rate of 50 mV s^{-1} at 25 °C. For clarity, only positive-scan CVs are shown.

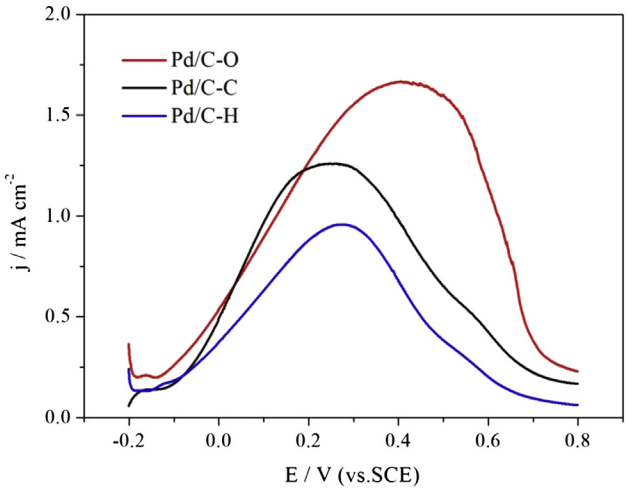

Fig. 4. CVs of different catalysts in 0.5 M H_2SO_4 + 0.5 M HCOOH solution with a scan rate of 50 mV s^{-1} at 25 °C. For clarity, only positive-scan CVs are shown.

Pd/C–C and Pd/C–H catalysts. The average particle sizes, calculated from the Pd (220) peak according to the Scherrer formulas [28] for the Pd/C–C, Pd/C–O and Pd/C–H catalysts are 4.1 nm, 4.7 and 4.4 nm, respectively.

The XPS was used as a primary tool to characterize the chemical composition of catalyst. According to the high-resolution spectra of Pd 3d for the Pd/C–O catalyst (Fig. 7(a)), the peaks at 334.40 and 339.65 eV are ascribed to metallic Pd, while the peaks at 336.05 and 341.20 eV are assigned to Pd (II) species; for Pd/C–C catalyst (Fig. 7(b)), the peaks at 335.15 and 340.40 eV are ascribed to metallic Pd, while the peaks at 336.80 and 342.05 eV are assigned to Pd (II) species; for Pd/C–H catalyst (Fig. 7(c)), the peaks at 336.05 and 341.25 eV are ascribed to metallic Pd, while the peaks at 336.95 and 342.25 eV are assigned to Pd (II) species. For Pd/C–O catalyst, Pd (II) negative shift evidently. More oxygen atoms were introduced in the Pd/C–O catalyst after the O_2 heat treatment, compared with the raw Pd/C–C catalyst. The electron density of per Pd atom will increase on the surface of Pd/C–O catalyst due to the electron transfer from O to Pd, which leads to the decreased electron binding energy of all the Pd atoms for the Pd/C–O catalyst. Apparently, the percentage composition of Pd (II) species in Pd/C–C

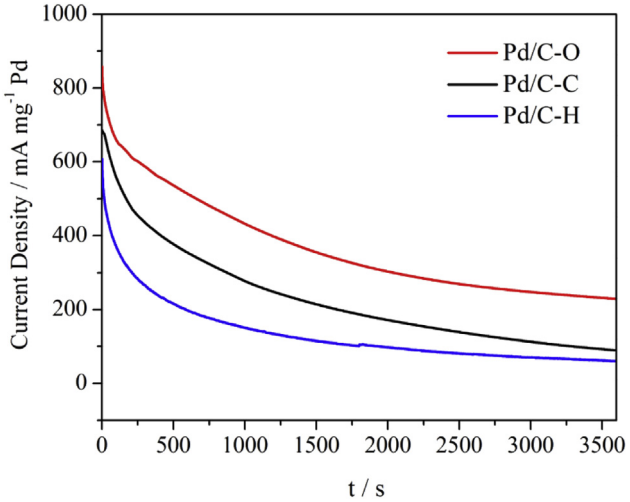

Fig. 5. Chronoamperometric curves of different catalysts in 0.5 M H_2SO_4 + 0.5 M HCOOH solution at 0.2 V at 25 °C.

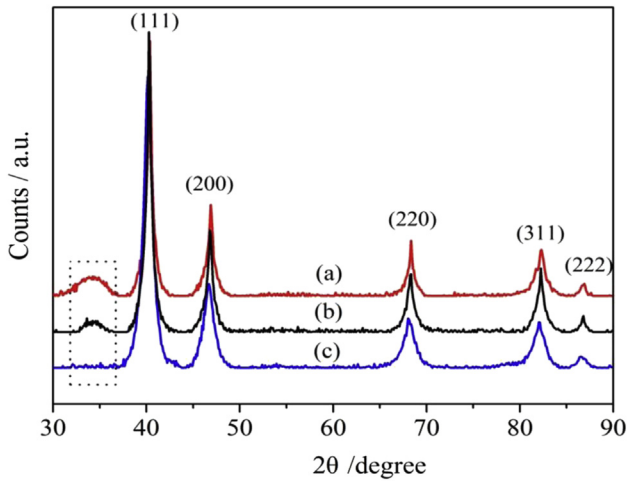

Fig. 6. XRD patterns for catalysts Pd/C–O (a), Pd/C–C (b) and Pd/C–H (c).

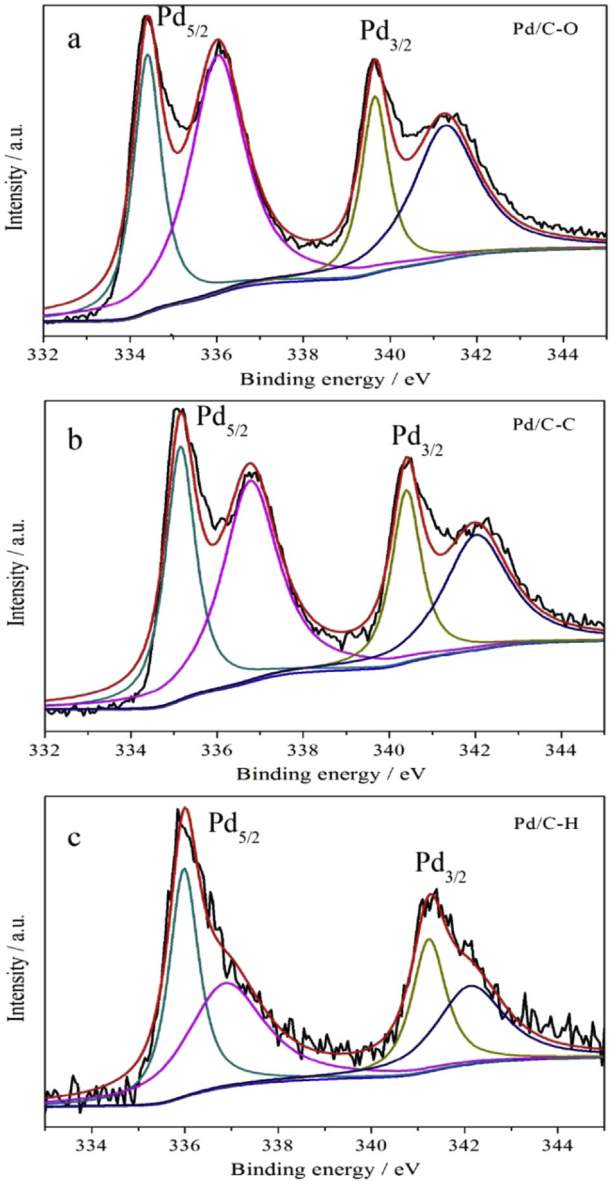

Fig. 7. High-resolution XPS spectra of Pd 3d for Pd/C–O (a), Pd/C–C (b) and Pd/C–H (c).

Table 2
The percentage composition of Pd (II) species.

Sample	Pd/C–C	Pd/C–O	Pd/C–H
Pd (II) (%)	53.04%	69.81%	30.46%

and Pd/C–H catalysts is lower than that in Pd/C–O catalyst, which is consistent with the above results of XRD, indicating that the Pd/C–O catalyst contains more POHOs [29]. The percentage composition of Pd (II) species of three catalysts are shown in Table 2.

Fig. 8 shows the TEM images of the different catalysts and the corresponding particle size distribution histograms. The O_2 and H_2 heat treatments on the Pd/C catalysts result in some extent of structural and surface changes on the catalysts. The aggregation of the Pd nanoparticles in Pd/C–O catalyst was serious, while the dispersion of the Pd nanoparticles in Pd/C–H catalyst was not uniform accompanying with some degree of aggregation. The major size distributions of Pd nanoparticles for Pd/C–O (Fig. 8C) and Pd/C–H (Fig. 8D) are 3.5–9 nm and 3–8.75 nm, respectively. The average particle sizes of Pd nanoparticles in the Pd/C–O, Pd/C–H catalysts are approximately 5.0 and 4.7 nm, respectively. This result is consistent with the size calculated from the XRD data (Fig. 9).

3.3. Performance and stability test of the single passive DFAFCs

Performance comparisons of three passive DFAFCs using different catalysts are shown in Fig. 8. Fig. 8(A) shows that the maximal power densities of the passive DFAFCs with Pd/C–O, Pd/

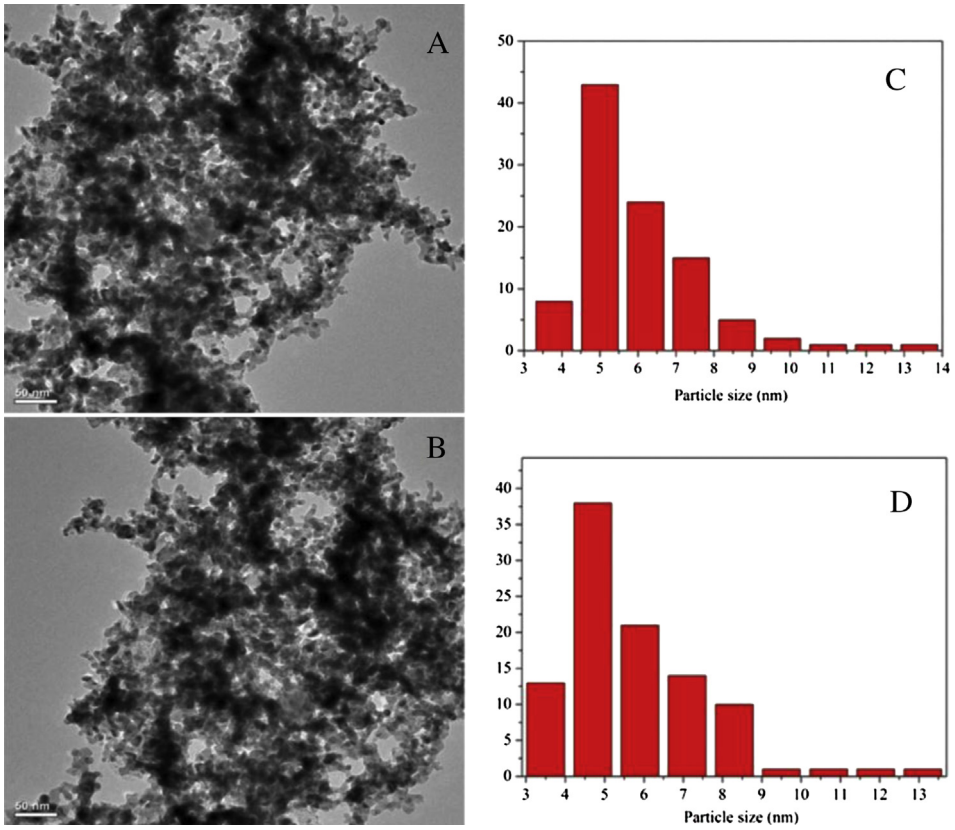

Fig. 8. TEM images of the catalysts and the corresponding particle size distribution histograms: Pd/C–O (A, C), Pd/C–H (B, D). The average particle size and corresponding size distributions were obtained by measuring the size of 100 randomly selected particles in the magnified TEM images.

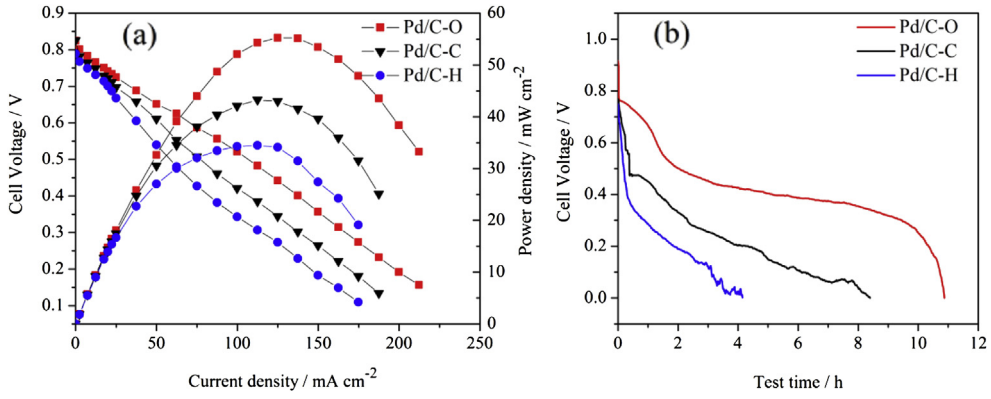

Fig. 9. Polarization and long-term constant-current discharge curves of the passive DFAFCs using Pd/C–O, Pd/C–C and Pd/C–H catalyst as anodes.

C–C and Pd/C–H anodic catalysts are 55.25 mW cm^{-2}, 42.38 mW cm^{-2} and 34.50 mW cm^{-2}, respectively. Fig. 8(B) shows the constant-current discharge curves of the passive DFAFCs at 50 mA cm^{-2} in 7.5 ml of 10 M HCOOH solution. The DFAFCs show different discharged performance as different anode catalysts are used, the passive DFAFC using Pd/C–O catalyst shows the highest output voltage and the longest discharged time during the whole operation of the cell. These results indicate that the introduction of POHOs significantly improves the performance of the DFAFCs, in which POHOs play a crucial role in enhancing the cell performance and decreasing cell degradation rate.

How the POHOs improve the catalyst performance is mainly resulted from the decrease in degradation rate of the catalyst, while the degradation of the catalyst performance is mainly caused from the poisoning of the catalysts. During the oxidation process of formic acid, the reaction intermediate CO is a major poisoning agent. The mitigation of the poisoning effect can only be acquired when the CO intermediate is effectively removed by oxidation. The POHOs provides the catalyst with abundant oxygen species, which is crucial for the CO removal through bifunctional mechanism, thereby increasing the stability of the catalyst due to the capability of removing CO at lower potentials. As a result, the Pd/C–O catalyst possesses the highest catalytic activity and stability.

4. Conclusions

In summary, the electrocatalytic activity and stability of the Pd/C–O catalyst for FAEO are enhanced greatly compared with the commercial Pd/C and Pd/C–H catalysts due to the introduction of POHOs. The high current density and high stability observed for FAEO confirm that the poisoning effect is largely decreased by the addition of POHOs into the Pd/C catalyst. The experimental results indicate that the Pd/C–O catalyst has great application prospect as a high-performance anode catalyst for DFAFCs.

Acknowledgments

This work was supported by the High Technology Research Program (863 program, nos. 2012AA053401) of the Science and Technology Ministry of China, National Basic Research Program of China (973 Program, nos. 2012CB932800 and 2012CB215500), General Programs of National Natural Science Foundation of China (21073180, 21011130027) and the *Recruitment Program of Foreign Experts* (WQ20122200077).

References

[1] C. Rice, S. Ha, R.I. Masel, P. Waszczuk, A. Wieckowski, T. Barnard, J. Power Sources 111 (2002) 83–89.
[2] C. Rice, S. Ha, R.I. Masel, A. Wieckowski, J. Power Sources 115 (2003) 229–235.
[3] Y. Zhu, Su Y. Ha, R.I. Masel, J. Power Sources 130 (2004) 8–14.
[4] S. Ha, R. Larsen, Y. Zhu, R.I. Masel, Fuel Cells 4 (2004) 337–343.
[5] N.V. Rees, R.G. Compton, J. Solid State Electrochem. 15 (2011) 2095–2100.
[6] X. Yu, P.G. Pickup, J. Power Sources 187 (2009) 493–499.
[7] X.W. Yu, P.G. Pickup, Electrochem. Commun. 11 (2009) 2012–2014.
[8] W.S. Jung, J. Han, S.P. Yoon, S.W. Nam, T.H. Lim, S.A. Hong, J. Power Sources 196 (2011) 4573–4578.
[9] M. Arenz, V. Stamenkovic, T.J. Schmidt, K. Wandelt, P.N. Ross, N.M. Markovic, Phys. Chem. Chem. Phys. 5 (2003) 4242–4251.
[10] W.P. Zhou, A. Lewera, R. Larsen, R.I. Masel, P.S. Bagus, A. Wieckowski, J. Phys. Chem. B 110 (2006) 13393–13398.
[11] C. Bianchini, P.K. Shen, Chem. Rev 109 (2009) 4183–4206.
[12] R. Larsen, S. Ha, J. Zakzeski, R.I. Masel, J. Power Sources 157 (2006) 78–84.
[13] J.L. Fernández, D.A. Walsh, A.J. Bard, J. Am. Chem. Soc 127 (2004) 357–365.
[14] S. Huang, S. Chang, C. Lin, C. Chen, C. Yeh, J. Phys Chem. B 110 (2006) 23300–23305.
[15] S. Huang, C. Chang, K. Wang, C. Yeh, ChemPhysChem 8 (2007) 1774–1777.
[16] Y. Wei, C. Liu, W. Chang, K. Wang, J. Alloys Compd. 509 (2011) 535–541.
[17] W. Wang, Y. Li, H. Wang, React. Kinet. Mech. Catal. 108 (2013) 433–441.
[18] S.H. Oh, G.B. Hoflund, J. Catal. 245 (2007) 35–44.
[19] M. Ren, Y. Kang, W. He, Z. Zou, X. Xue, D.L. Akins, H. Yang, S. Feng, Appl. Catal. B Environ. 104 (2011) 49–53.
[20] A. Capon, R. Parsons, J. Electroanal. Chem. (1973) 205–231.
[21] T. Kawaguchi, W. Sugimoto, Y. Murakami, Y. Takasu, Electrochem. Commun. 6 (2004) 480–483.
[22] Y. Takasu, T. Fujiwara, Y. Murakami, K. Sasaki, M. Oguri, T. Asaki, W. Sugimoto, J. Electrochem. Soc. 147 (2000) 4421–4427.
[23] L. Yan, J. Liao, L. Feng, X. Zhao, L. Liang, W. Xing, C. Liu, J. Electroanal. Chem. 688 (2013) 49–52.
[24] Y. Suo, I.M. Hsing, Electrochim. Acta 55 (2009) 210–217.
[25] Y.W. Lee, J.K. Oh, H.S. Kim, J.K. Lee, S.B. Han, W. Choi, K.W. Park, J. Power Sources 195 (2010) 5896–5901.
[26] D. Morales-Acosta, J. Ledesma-Garcia, L.A. Godinez, H.G. Rodríguez, L. Álvarez-Contreras, L.G. Arriaga, J. Power Sources 195 (2010) 461–465.
[27] E. Antolini, F. Cardellini, J. Alloys Compd. 315 (2001) 118–122.
[28] V. Radmilovic, H.A. Gasteiger, P.N. Ross, J. Catal. 154 (1995) 98–106.
[29] J. Chang, X. Sun, L. Feng, W. Xing, X. Qin, G. Shao, J. Power Sources 239 (2013) 94–102.